The International Journal of Robotics Research

http://ijr.sagepub.com/

Design and experimental evaluation of a dynamically balanced redundant planar 4-RRR parallel manipulator

Volkert van der Wijk, Sébastien Krut, François Pierrot and Just L Herder

The International Journal of Robotics Research 2013 32: 744
DOI: 10.1177/0278364913484183

The online version of this article can be found at:
http://ijr.sagepub.com/content/32/6/744

Published by:

http://www.sagepublications.com

On behalf of:

Multimedia Archives

Additional services and information for *The International Journal of Robotics Research* can be found at:

Email Alerts: http://ijr.sagepub.com/cgi/alerts

Subscriptions: http://ijr.sagepub.com/subscriptions

Reprints: http://www.sagepub.com/journalsReprints.nav

Permissions: http://www.sagepub.com/journalsPermissions.nav

Citations: http://ijr.sagepub.com/content/32/6/744.refs.html

>> Version of Record - Jun 7, 2013

What is This?

Downloaded from ijr.sagepub.com at Universiteit Twente on June 7, 2013

The International Journal of
Robotics Research
32(6) 744–759
© The Author(s) 2013
Reprints and permissions:
sagepub.co.uk/journalsPermissions.nav
DOI: 10.1177/0278364913484183
ijr.sagepub.com

Design and experimental evaluation of a dynamically balanced redundant planar 4-RRR parallel manipulator

Volkert van der Wijk[1], Sébastien Krut[2], François Pierrot[2] and Just L Herder[1]

Abstract

Shaking forces and shaking moments in high-speed parallel manipulators are a significant cause of base vibrations. These vibrations can be eliminated by designing the manipulator to be shaking-force balanced and shaking-moment balanced. In this article an approach for the design and evaluation of high-speed dynamically balanced parallel manipulators is presented and applied to a comparative experimental investigation of a balanced and unbalanced DUAL-V planar 4-RRR parallel manipulator. For precise simulation of the manipulator motion, the inverse dynamic model of the manipulator is derived and validated.

Experiments show that the balanced manipulator has up to 97% lower shaking forces and up to a 96% lower shaking moment. For small inaccuracies of the counter-masses or for a small unbalanced payload on the platform, base vibrations may be considerable for high-speed manipulation, however their values remain significantly low as compared to the unbalanced manipulator. For the balanced manipulator the actuator torques are about 1.6 times higher and the bearing forces are about 71% lower as compared to the unbalanced manipulator.

Keywords

Shaking force balancing, shaking moment balancing, parallel manipulator, actuator torques, bearing forces, experiments

1. Introduction

During recent decades parallel manipulators (i.e. robots) have found their way into industry for applications such as fast pick-and-place tasks. The continuous demand for increased operational speeds of these robots has challenged designers with various issues. One of them is the severe vibration in the base due to shaking forces and shaking moments, i.e. the inertial forces and moments exerted by the manipulator on the base, in practice, a major cause of wear and failure of the manipulator, its control system, and neighboring machines. Common solutions to reducing the influence of these vibrations include increasing the stiffness and mass of the base, applying damping, and by sophisticated control. Another solution, that eliminates the source of vibration at its roots, is to design the parallel manipulator such that, for all motion, the shaking forces and the shaking moments are minimal or zero. Such a manipulator is said to be dynamically balanced and is characterized by having both the sum of the linear momentum, and the sum of the angular momentum of all its elements constant for all motion (Van der Wijk et al., 2009).

Contrary to the dynamic balancing of mechanisms, a topic that has been investigated for well over a century (Arakelian and Smith, 2005a, 2005b), the dynamic balancing of manipulators, and in particular the dynamic balancing of parallel manipulators started relatively recently. The shaking-force balancing of the serial manipulator PUMA-760 was studied at the end of the 1980s by Chung and Cho (1988) and Lim et al. (1989, 1990). In 1996 the shaking-force balancing of a three-degree-of-freedom (3-DoF) planar parallel manipulator was investigated by Jean and Gosselin (1996). In 2000 the dynamic balancing of parallel manipulators was first treated in a more general way by Ricard and Gosselin (2000). Although various articles have been published since, the total volume of related literature is considerably small. In addition, most of the literature investigates the balancing of multi-DoF manipulators by application of balance solutions for mechanisms, which has shown to have a number of disadvantages regarding additional mass, inertia, and complexity (Van der Wijk et al.,

[1]Laboratory of Mechanical Automation and Mechatronics, University of Twente, The Netherlands
[2]Le Laboratoire d'Informatique, de Robotique et de Microélectronique, Montpellier, France

Corresponding author:
Just L Herder, Laboratory of Mechanical Automation and Mechatronics, University of Twente, PO Box 217, Enschede 7500, The Netherlands.
Email: j.l.herder@utwente.nl

Downloaded from ijr.sagepub.com at Universiteit Twente on June 7, 2013

2009). Recently, balance solutions that take advantage of the parallel structure of manipulators were shown to have significant potential (Van der Wijk et al., 2011; Van der Wijk and Herder, 2012a, 2012b).

Also most literature on dynamic balancing, both for mechanisms and for manipulators, is theoretical, there are relatively few experimental results. Regarding serial manipulators, in Chung and Cho (1988) the experiments on the PUMA-760 showed that shaking-force balancing reduced the actuator torques significantly since actuators do not have to compensate gravity forces. The inertia increased with balancing, but it was found that the actuator torques due to Coulomb friction dominated, for which the inertia increase was found acceptable. Because of lower actuator torques, in Lim et al. (1989) it was experimentally shown that shaking-force balancing is advantageous for the accuracy of the dynamic identification of the unbalanced robot. The balanced PUMA-760 also had a nine times higher payload capacity, or the ability to move at double acceleration and at about three times higher velocities (Lim et al., 1990).

Regarding parallel manipulators, in Agrawal et al. (2001) a shaking-force balanced parallel mechanism based on the principal vector linkage of Fischer (1906) was presented and tested. Although presented as a balanced serial chain, it can be regarded as a force-balanced parallel manipulator. The center-of-mass (CoM) of the linkage is an invariant point in one of the joints, which was verified by moving the mechanism in a statically balanced way while measuring the joint angles.

In Foucault and Gosselin (2004) a dynamically balanced 3-DoF planar parallel manipulator was presented and tested. The manipulator was composed of two independently force-balanced parallelograms pivoted to the base and coupled with an end-effector link. Shaking-moment balancing was achieved with separate counter-rotating inertias (inertia-wheels). The manipulator was suspended by vertical cables which allowed it to float within the horizontal plane and it was actuated at a low speed, corresponding to the eigenmotion of this suspension. The motion of a point in the base of the manipulator was measured to verify the balance performance.

The goal of this article is to present an approach for the design and evaluation of high-speed dynamically balanced parallel manipulators, and to apply this approach for a comparative experimental investigation of the balanced and the unbalanced DUAL-V planar 4-RRR parallel manipulator.

In addition to the balance performance, other important aspects such as the influence of the balance elements on the actuator torques and on the bearing forces are investigated. In addition, the sensitivity of the balance parameters and the influence of payload are evaluated.

First the design and evaluation approaches are presented followed by the detailed design of the balanced DUAL-V manipulator. For this manipulator, the exact inverse dynamic model is derived and validated and used for precise simulations without the need of a controller. The experimental setup and the experiments are described and the experimental results are presented and discussed.

2. Approach to the design and evaluation of a balanced manipulator

This section presents and discusses approaches to the design and evaluation of high-speed balanced parallel manipulators, which are applied to investigation of the planar 4-RRR parallel manipulator.

2.1. Design

To take advantage of the parallel architecture for the purpose of dynamic balance, the common way of balancing – to first consider solely the kinematics of the manipulator and subsequently its balancing – is not effective and efficient. When, after all the effort to balance a given architecture, the balance solutions are not applicable, the kinematics will have to be considered all over again. Considering the balance properties at the very beginning of the kinematic design is therefore essential. In Demeulenaere and Berkof (2008) suggestions in this direction were proposed for the field of input-torque balancing of machines. Moreover, for multi-DoF manipulators the kinematics are often not as influential as they are for single-DoF mechanisms. Although for example, the useful workspace of a manipulator depends on the kinematic design, often a wide variety of kinematic designs is applicable to carrying out the intended tasks. Especially with the target of high-speed manipulators, this should be used to our advantage.

Since for dynamic balance, the sum of the linear momentum and the sum of the angular momentum of all manipulator elements needs to be constant, dynamic balance is all about similar opposite motion of masses and inertias. This means that from a kinematic point of view elements need to counter-rotate and to counter-move with respect to one another. The more the motions are similar and opposite, the better the balanced solution can be. The level of similar opposite motion depends on the mass distribution in each element. Additional balance elements such as countermasses and counter-inertias can be advantageous for tuning the mass distributions. However for low mass, low inertia, and low complexity they should only be applied to elements connecting the base (Van der Wijk and Herder, 2009).

The design of a balanced manipulator can be approached in two ways. If an initial kinematic architecture of the manipulator is known, the kinematic parameters can be adapted by rearranging the locations of the base pivots and by changing the dimensions of the elements to induce and to improve counter-motion of elements. Accordingly, the mass distributions can be adapted to induce and improve balance. This means that both the kinematic parameters and the mass parameters in the equations of the linear momentum and the angular momentum are adapted. With this approach it is

Downloaded from ijr.sagepub.com at Universiteit Twente on June 7, 2013

also possible to obtain the best compromises between kinematics and balance, especially when perfect balance is not required.

A second approach is to derive balanced manipulators from known balanced architectures such as (pantograph-based) principal vector linkages (Van der Wijk and Herder, 2012b) or other inherently balanced linkages (Van der Wijk and Herder, 2012a). These architectures are based on the essential kinematic relations for balance and as long as these relations are maintained, any manipulator that is derived is balanced. This approach is specifically interesting for synthesis of a wide variety of kinematic solutions with perfect balance capability. Both approaches will be employed for the balancing of the planar 4-RRR parallel manipulator.

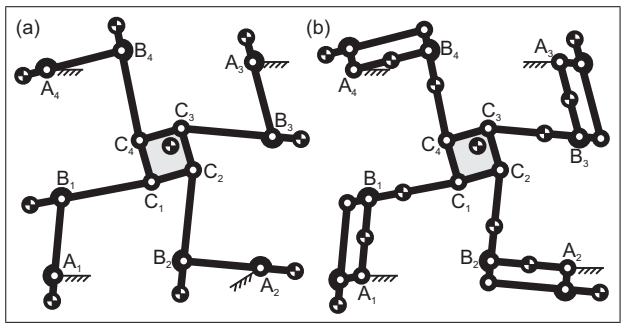

Fig. 1. A planar 4-RRR manipulator with the common force-balance principle of having the CoM of each of the four arms with part of the platform mass in fixed pivots A_i with (a) counter-masses in each link of the arms and with (b) pantograph arms with a counter-mass.

2.2. Evaluation and comparative study

To verify if theoretical results are correct, the first step of the evaluation of the balanced manipulator is to measure the balance performance. The shaking forces and shaking moments can be obtained from a multi-body simulation with an accurate model of the prototype manipulator or from measurements in an experimental setup. From the fabrication process of the prototype manipulator and from the obtained balance precision, the costs of the balance solution in terms of structural design and production effort can be derived together with the sensitivity to balance inaccuracies. For the potential of the manipulator it is important to also investigate and measure the required driving power (actuator torques) and the bearing forces, which determine the structural demand on the design, e.g. the size of the actuators and the stiffness of the system.

For both the evaluation and the comparative investigation, it is important to exclude the influence of the controller and the control design. Although a controller is required to move the manipulator and in practice it will never move the manipulator exactly as desired, the shaking forces and shaking moments do not depend on the controller directly. They depend solely on the actual motion of the manipulator. This means that even with a bad controller the balance performance can be evaluated well when the real motion of the manipulator is considered and measured and also is used as input in the simulations.

To validate the measured results, the measured manipulator motion can be simulated precisely with a multi-body dynamic model when the exact inverse dynamics are known. Then the design of a controller for the simulation is omitted since open-loop control can be applied, calculating the required actuator torques at each time step.

Also the bearing forces do not depend on the controller directly but they depend on the real motion of the manipulator. In practice it is challenging to measure the bearing forces in an experimental setup but they can be estimated from a precise simulation of the measured manipulator motion.

3. Design of the DUAL-V manipulator

In this section the two design approaches are applied for the synthesis of a balanced redundant 3-DoF planar 4-RRR parallel manipulator. Figure 1(a) shows the typical design of a 3-DoF planar 4-RRR parallel manipulator which consists of four 2-DoF arms (or dyads) i connecting the moving platform (or end-effector) $C_1C_2C_3C_4$ with four pivots A_i to the fixed base. With an actuator in each of the four fixed pivots, the manipulator has one degree of actuation redundancy. This is advantageous since manipulators with actuation redundancy have an increased acceleration capability and have more homogeneous dynamic characteristics (e.g. force transmission to the platform) throughout the workspace (Corbel et al., 2010).

Figures 1(a) and (b) show how this manipulator is force balanced when common balance principles for mechanisms are applied. For the balance solution in Figure 1(a) the CoM of each link B_iC_i is located such that the CoM of this link together with part of the platform mass modeled in C_i is in B_i, and the CoM of each link A_iB_i is located such that the CoM of this link together with both the mass of link B_iC_i and part of the platform mass modeled in B_i is in A_i, which can be achieved with additional counter-masses in each of the links (Van der Wijk et al., 2011). In Figure 1(b) each of the four arms is balanced with a single counter-mass and additional parallel links which therefore result in pantograph linkages of which the CoM of the links, counter-mass, and part of the platform mass is in A_i (Van der Wijk and Herder, 2008; Briot et al., 2009). This solution proved to be advantageous for low mass and low inertia at the cost of increased complexity (Van der Wijk et al., 2009).

Instead of adding a parallelogram to each of the four arms as in Figure 1(b), the arms can also be designed and arranged such that two pairs of arms each form a parallelogram as shown in Figure 2(a). When the manipulator moves, the parallelograms are maintained for all translations throughout the workspace when the platform is not rotated. This solution can be derived from the linear momentum equations of the manipulator (Van der Wijk

Downloaded from ijr.sagepub.com at Universiteit Twente on June 7, 2013

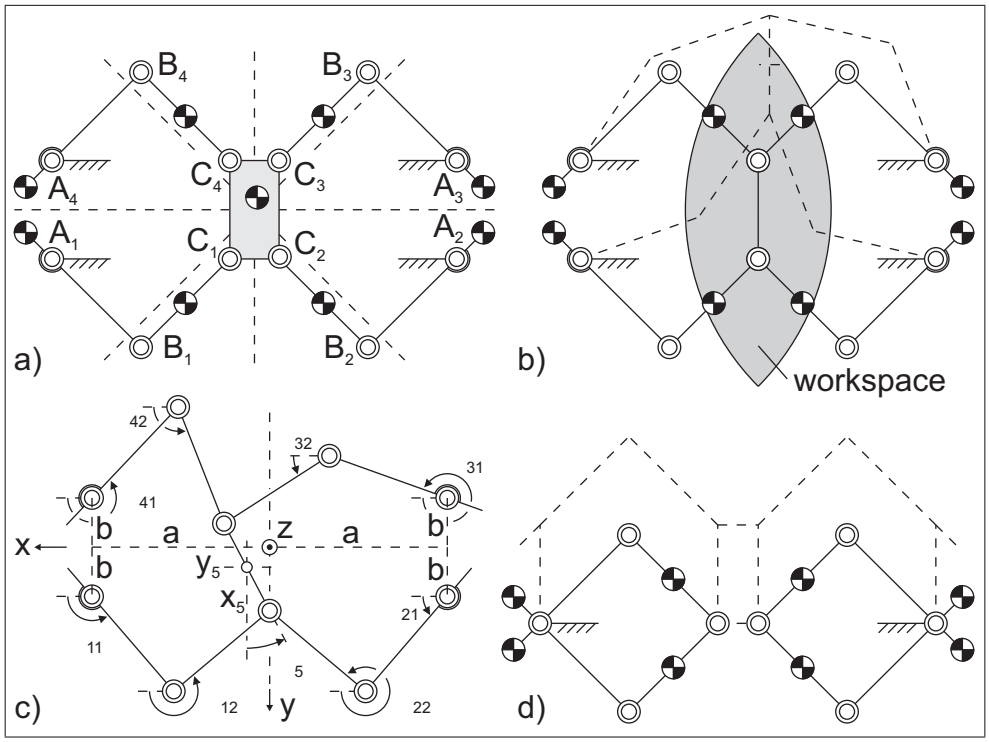

Fig. 2. (a) Specific kinematic solution such that for the translational motion of a non-rotated platform, force-balance is obtained solely with counter-masses in elements connecting the base; (b) Compact DUAL-V configuration where the platform joints coincide; (c) Definition of the kinematic variables and the parameters of the base; (d) Synthesis of the DUAL-V configuration from two force-balanced pantographs.

et al., 2011), which for force balance are constant. Since the motion of parallel links is linearly related, the linear momentum equations are reduced and result in a force-balanced solution where each pair of arms is balanced with two counter-masses in the links connecting the base. Then the 4-RRR manipulator can be force balanced with four counter-masses in total.

For a platform rotation ($\theta_5 \neq 0$) the parallelograms are not maintained. This means that motion with a rotated platform is not perfectly force balanced. Since for rotations of the platform the pairs of arms remain close to a parallelogram, the force balance still can be expected to be advantageous.

Because of the symmetric kinematic design, when the 4-RRR manipulator moves along the orthogonal axes without rotation, all links connecting the base counter-rotate linearly with one another and also all links connecting the platform counter-rotate linearly with one another. This means that when the links in each of these two groups have equal inertia, they balance out their shaking moments and the manipulator then is also perfectly shaking-moment balanced for these motions. For motion with a non-rotated platform along the diagonal axes, the links counter-rotate almost linearly with one another and the manipulator is almost perfectly shaking-moment balanced for these motions. To have four arms instead of the minimum of three arms for a 3-DoF manipulator therefore is not only beneficial for actuation redundancy, but also to obtain a symmetric kinematic and dynamic design that is beneficial for dynamic balance. Motion with a rotated platform or off the orthogonal axes is not perfectly moment balanced. Since the motion remains in the vicinity of perfect dynamic balance, also here the balance performance can be expected to be advantageous.

For improved force transmission to the platform and for compactness of the manipulator, the platform can be reduced to a link with coinciding joints as shown in Figure 2(b). This configuration is named the 'DUAL-V' manipulator.

The synthesis so far is based on the first design approach of adapting the kinematic parameters and the mass parameters of an initial kinematic architecture. Synthesis based on the second approach is illustrated in Figure 2(d). Here the DUAL-V configuration is composed of two force-balanced pantographs, i.e. composed of known balanced architectures which can be adapted to the DUAL-V design without affecting the balance capabilities of the pantographs. This is since pantographs keep their balance properties for any adaption as long as the parallelograms are maintained for all motion.

A prototype of the DUAL-V manipulator was designed and fabricated with the parameters in Table 1. These parameters and the kinematic variables of the manipulator are illustrated in Figure 2(c) and Figure 3, of which the latter shows the top-view of the computer-aided design (CAD) of the prototype manipulator. All arm links $i1$ and $i2$ have equal lengths l_{i1} and l_{i2}, respectively, the fixed pivots are

Downloaded from ijr.sagepub.com at Universiteit Twente on June 7, 2013

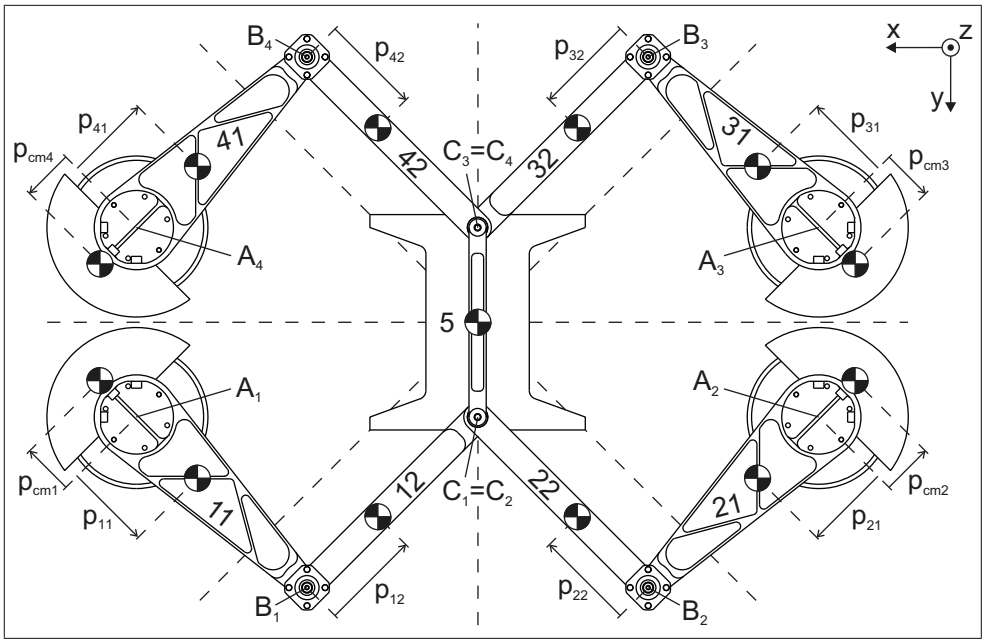

Fig. 3. Computer-aided design of a DUAL-V prototype manipulator with parameter definitions (patent pending).

located at distances $a = l_{i1}\sqrt{2}$ and b with respect to the center, and the platform link 5 has a length $l_5 = 2b$. With these parameters the pairs of arms are parallelograms for motion along the orthogonal axes with a non-rotated platform. The theoretical workspace of the manipulator for the given dimensions is shown in Figure 2(b) and consists of the intersection of two circles with radii $l_{i1} + l_{i2} = 0.56$ m of which the maximal width along x is $2(l_{i1} + l_{i2} - a) = 0.328$ m and the maximal width along y is $2\sqrt{(l_{i1} + l_{i2})^2 - a^2} = 2a = 0.792$ m. Due to collisions, the motion of the prototype along x is limited to a workspace width of 0.288 m.

The links of the manipulator are made of aluminium and were designed and produced before the counter-masses. Together with all bolts, nuts, bearings, etc. they were measured with a 0.01 mm accurate digital caliper and weighed with a 0.01 g accurate balance. Together with the CAD model in SolidWorks the parameters of the link CoMs p_{i1} and p_{i2}, the masses of the links m_{i1}, m_{i2}, and m_5, and their inertia about their CoM I_{i1}, I_{i2}, and I_5 were determined.

Subsequently the counter-masses were designed from circular segments made of brass. Their required mass $m_{\mathrm{cm},i}$ and CoM location at distance $p_{\mathrm{cm},i}$ relative to A_i were calculated with the force-balance conditions which for the first design approach were derived from (Van der Wijk et al., 2011) as

$$\begin{aligned}
&m_{11}p_{11} + m_{12}l_{11}\left(1 - \frac{p_{12}}{l_{12}}\right) + m_{42}p_{42} + m_{32}l_{42}\frac{p_{32}}{l_{32}} \\
&\quad + m_5\frac{l_{42}}{2} = m_{\mathrm{cm},1}p_{\mathrm{cm},1} \\
&m_{21}p_{21} + m_{22}l_{21} + m_{12}l_{21}\frac{p_{12}}{l_{12}} + \frac{m_5}{2}l_{21} \\
&\quad = m_{\mathrm{cm},2}p_{\mathrm{cm},2} \qquad (1) \\
&m_{31}p_{31} + m_{32}l_{31}\left(1 - \frac{p_{32}}{l_{32}}\right) + m_{22}p_{22} + m_{12}l_{22}\frac{p_{12}}{l_{12}} \\
&\quad + m_5\frac{l_{22}}{2} = m_{\mathrm{cm},3}p_{\mathrm{cm},3} \\
&m_{41}p_{41} + m_{42}l_{41} + m_{32}l_{41}\frac{p_{32}}{l_{32}} + \frac{m_5}{2}l_{41} \\
&\quad = m_{\mathrm{cm},4}p_{\mathrm{cm},4}
\end{aligned}$$

and from the second design approach were derived from (Van der Wijk and Herder, 2012b) as

$$\begin{aligned}
m_{11}p_{11} + m_{12}l_{11} + m_{42}p_{42} + m_5\tfrac{l_{11}}{2} &= m_{\mathrm{cm},1}p_{\mathrm{cm},1} \\
m_{21}p_{21} + m_{22}l_{21} + m_{32}p_{32} + m_5\tfrac{l_{21}}{2} &= m_{\mathrm{cm},2}p_{\mathrm{cm},2} \\
m_{31}p_{31} + m_{32}l_{31} + m_{22}p_{22} + m_5\tfrac{l_{31}}{2} &= m_{\mathrm{cm},3}p_{\mathrm{cm},3} \\
m_{41}p_{41} + m_{42}l_{41} + m_{12}p_{12} + m_5\tfrac{l_{41}}{2} &= m_{\mathrm{cm},4}p_{\mathrm{cm},4}
\end{aligned} \qquad (2)$$

which both give equal results.

The main aim of the design of the counter-masses was to have the reduced inertia $I_{\mathrm{cm},i} + m_{\mathrm{cm},i}p_{\mathrm{cm},i}^2$ of each counter-mass relative to A_i be as low as possible since this is advantageous for low actuator torques (Van der Wijk et al., 2012). Therefore a high mass of each counter-mass with its CoM as close to A_i as possible is needed. A counter-mass material with high density such as brass and a design which can be large in the out-of-plane direction (thick counter-masses are advantageous. The design of the counter-masses was verified with the mass properties function in SolidWorks, with which it was also verified that the common CoM of the complete manipulator is at the same location for any position in the workspace with a non-rotated platform.

Each counter-mass was designed such that part of its mass $m_{\mathrm{tun},i} = 0.188$ kg is a separate element made of lead, placed at a distance $p_{\mathrm{tun},i} = 0.080$ m from A_i on top of the brass segments. This was done to fine-tune the counter-masses, compensating for production inaccuracies and to be

Downloaded from ijr.sagepub.com at Universiteit Twente on June 7, 2013

Table 1. DUAL-V parameters.

[m]	[kg]	[kgm^2]	[m]
$l_{i1} = 0.2800$	$m_{i1} = 1.169$	$I_{i1} = 0.012967$	$p_{i1} = 0.0737$
$l_{i2} = 0.2800$	$m_{i2} = 0.606$	$I_{i2} = 0.006417$	$p_{i2} = 0.1279$
$l_5 = 0.2200$	$m_5 = 0.899$	$I_5 = 0.008168$	$p_{\mathrm{cm},i} = 0.0575$
$a = 0.3960$	$m_{\mathrm{cm},i} = 7.983$	$I_{\mathrm{cm},i} = 0.026845$	$p_{\mathrm{tun},i} = 0.080$
$b = 0.1100$	$m_{\mathrm{tun},i} = 0.188$	$I_{\mathrm{act},i} = 0.004100$	

able to remove a small mass for experiments investigating the balance performance with non-perfect counter-masses. The mass and inertia of these tuning masses are included in the parameters $m_{\mathrm{cm},i}$ and $I_{\mathrm{cm},i}$ in Table 1.

4. Inverse dynamic model and validation with simulation model

In this section the inverse dynamic model of the DUAL-V is derived and validated with a multi-body simulation.

4.1. Inverse dynamic model to derive the actuator torques

The motion of the platform of the DUAL-V can be prescribed with $\overline{u} = [x_5(t), y_5(t), \theta_5(t)]^T$ with the position of the center of the platform (x_5, y_5) and the orientation of the platform θ_5 relative to the xy-reference frame at a time t, as illustrated in Figure 2(c). The actuator torques $\overline{\tau}$ required at a time t for a prescribed motion $\overline{u}$ can be calculated as a combination of three individual parts as

$$\overline{\tau} = \overline{\tau}_I + \overline{\tau}_{II} + \overline{\tau}_{III}. \tag{3}$$

Here $\overline{\tau}_I$ is the required actuator torque to move the platform and part of the mass of links $i2$, $\overline{\tau}_{II}$ is the required actuator torque to move links $i1$ and part of the mass of links $i2$, and $\overline{\tau}_{III}$ is the required actuator torque of part of the rotational motion of links $i2$. This approach follows from Corbel et al. (2010) and is extended to being exact by not simplifying the dynamics of the links $i2$. Similar to Corbel et al. (2010), the mass of links $i2$ is distributed equivalently to joints B_i and C_i and is included in both $\overline{\tau}_I$ and $\overline{\tau}_{II}$. However the rotational inertia of links $i2$ then is not completely considered. $\overline{\tau}_{III}$ therefore is the torque required to include the rotational inertia of links $i2$ exactly, as will become clear later on.

4.1.1. Actuator torques $\overline{\tau}_I$ for the motion of the platform The actuator torques $\overline{\tau}_I$ for the motion of the platform can be calculated from the equations of the power of the actuator torques $\overline{\tau}_I$ that has to be equal to the power of the motion of the platform, which is written as

$$\dot{\overline{q}}^T \overline{\tau}_I = \dot{\overline{u}}^T \overline{F}_{\mathrm{p}} \tag{4}$$

where $\dot{\overline{q}} = [\dot{\theta}_{11}, \dot{\theta}_{21}, \dot{\theta}_{31}, \dot{\theta}_{41}]^T$ is the vector of the angular velocities of the driven links $i1$, $\dot{\overline{u}} = [\dot{x}_5, \dot{y}_5, \dot{\theta}_5]^T$ is the vector of the velocities of the platform motion, and $\overline{F}_{rmp}$ is the vector of the resultant forces and the resultant moment that act on the platform. For a prescribed motion of the platform, $\dot{\overline{q}}$ can be derived from the velocity vectors of joints B_i and C_i along the line B_iC_i which, for a rigid link, are equal. These vectors are shown in Figure 4(a) and are written and calculated as

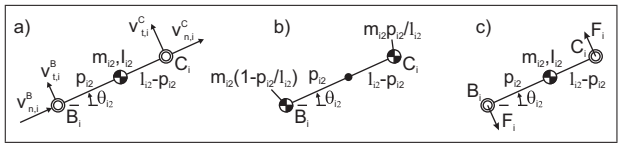

Fig. 4. (a) Velocity vectors of joints B_i and C_i of links $i2$; (b) Equivalent mass model of links $i2$; (c) Forces F_i in joints B_i and C_i for rotational acceleration of links $i2$.

$$v^B_{n,i} = v^C_{n,i} \quad \rightarrow \quad \overline{X}_n \dot{\overline{q}} = \overline{Y}_n \dot{\overline{u}} \tag{5}$$

with

$$\overline{X}_n = \begin{bmatrix} -l_{11}s(\theta_{11}-\theta_{12}) & 0 & 0 & 0 \\ 0 & -l_{21}s(\theta_{21}-\theta_{22}) & 0 & 0 \\ 0 & 0 & -l_{31}s(\theta_{31}-\theta_{32}) & 0 \\ 0 & 0 & 0 & -l_{41}s(\theta_{41}-\theta_{42}) \end{bmatrix} \tag{6}$$

$$\overline{Y}_n = \begin{bmatrix} c(\theta_{12})\, s(\theta_{12}) & -c(\theta_{12}-\theta_5)\, b \\ c(\theta_{22})\, s(\theta_{22}) & -c(\theta_{22}-\theta_5)\, b \\ c(\theta_{32})\, s(\theta_{32}) & c(\theta_{32}-\theta_5)\, b \\ c(\theta_{42})\, s(\theta_{42}) & c(\theta_{42}-\theta_5)\, b \end{bmatrix}. \tag{7}$$

Here $s(\,)$ and $c(\,)$ are used as shorthand notation for sin( ) and cos( ), respectively, and b is the parameter in Table 1. From equation (5) $\dot{\overline{q}}$ then is derived as

$$\dot{\overline{q}} = \overline{X}_n^{-1} \overline{Y}_n \dot{\overline{u}} = \overline{J} \dot{\overline{u}} \tag{8}$$

in which $\overline{J}$ is the Jacobian matrix

$$\overline{J} = \begin{bmatrix} \frac{-c(\theta_{12})}{l_{11}s(\theta_{11}-\theta_{12})} & \frac{-s(\theta_{12})}{l_{11}s(\theta_{11}-\theta_{12})} & \frac{c(\theta_{12}-\theta_5)}{l_{11}s(\theta_{11}-\theta_{12})} b \\ \frac{-c(\theta_{22})}{l_{21}s(\theta_{21}-\theta_{22})} & \frac{-s(\theta_{22})}{l_{21}s(\theta_{21}-\theta_{22})} & \frac{c(\theta_{22}-\theta_5)}{l_{21}s(\theta_{21}-\theta_{22})} b \\ \frac{-c(\theta_{32})}{l_{31}s(\theta_{31}-\theta_{32})} & \frac{-s(\theta_{32})}{l_{31}s(\theta_{31}-\theta_{32})} & \frac{-c(\theta_{32}-\theta_5)}{l_{31}s(\theta_{31}-\theta_{32})} b \\ \frac{-c(\theta_{42})}{l_{41}s(\theta_{41}-\theta_{42})} & \frac{-s(\theta_{42})}{l_{41}s(\theta_{41}-\theta_{42})} & \frac{-c(\theta_{42}-\theta_5)}{l_{41}s(\theta_{41}-\theta_{42})} b \end{bmatrix}. \tag{9}$$

The resultant forces and the resultant moment on the platform can be calculated as $\overline{F}_{\mathrm{p}} = \overline{M}_I \ddot{\overline{u}}$, where $\ddot{\overline{u}} = [\ddot{x}_5, \ddot{y}_5, \ddot{\theta}_5]^T$ are the accelerations of the platform motion and $\overline{M}_I$ is the mass matrix

$$\overline{M}_I = \begin{bmatrix} m_5 + \sum_{i=1}^{4} m_{\mathrm{eq},i2} & 0 & 0 \\ 0 & m_5 + \sum_{i=1}^{4} m_{\mathrm{eq},i2} & 0 \\ 0 & 0 & I_5 + (\sum_{i=1}^{4} m_{\mathrm{eq},i2})\, b^2 \end{bmatrix} \tag{10}$$

with the equivalent masses $m_{\mathrm{eq},i2} = m_{i2}p_{i2}/l_{i2}$ of links $i2$ that are modeled in joints C_i as illustrated in Figure 4(b). From equation (4) $\overline{\tau}_I$ then is obtained as

$$(\overline{J}\dot{\overline{u}})^T \overline{\tau}_I = \dot{\overline{u}}^T \overline{M}_I \ddot{\overline{u}} \quad \Rightarrow \quad \overline{\tau}_I = \overline{J}^{T*} \overline{M}_I \ddot{\overline{u}} \tag{11}$$

with the pseudo-inverse Jacobian $\overline{J}^*$.

Downloaded from ijr.sagepub.com at Universiteit Twente on June 7, 2013

4.1.2. Actuator torques $\overline{\tau}_{II}$ for the motion of links $i1$ The actuator torques $\overline{\tau}_{II}$ for the motion of links $i1$ can be calculated with

$$\overline{\tau}_{II} = \overline{M}_{II}\ddot{\overline{q}} \tag{12}$$

with $\ddot{\overline{q}} = [\ddot{\theta}_{11}, \ddot{\theta}_{21}, \ddot{\theta}_{31}, \ddot{\theta}_{41}]^T$ the vector of the angular accelerations of the driven links $i1$ and with mass matrix $\overline{M}_{II}$ written as

$$\overline{M}_{II} = \begin{bmatrix} I_{11} + m_{11}p_{11}^2 + I_{\mathrm{cm},1} + m_{\mathrm{cm},1}p_{\mathrm{cm},1}^2 + I_{\mathrm{act},1} + m_{\mathrm{eq},11}l_{11}^2 & 0 & 0 & 0 \\ 0 & I_{21} + m_{21}p_{21}^2 + I_{\mathrm{cm},2} + m_{\mathrm{cm},2}p_{\mathrm{cm},2}^2 + I_{\mathrm{act},2} + m_{\mathrm{eq},21}l_{21}^2 & 0 & 0 \\ 0 & 0 & I_{31} + m_{31}p_{31}^2 + I_{\mathrm{cm},3} + m_{\mathrm{cm},3}p_{\mathrm{cm},3}^2 + I_{\mathrm{act},3} + m_{\mathrm{eq},31}l_{31}^2 & 0 \\ 0 & 0 & 0 & I_{41} + m_{41}p_{41}^2 + I_{\mathrm{cm},4} + m_{\mathrm{cm},4}p_{\mathrm{cm},4}^2 + I_{\mathrm{act},4} + m_{\mathrm{eq},41}l_{41}^2 \end{bmatrix} \tag{13}$$

which includes the inertias $I_{i1} + m_{i1}p_{i1}^2$ of links $i1$ about joints A_i, the inertias $I_{\mathrm{cm},i} + m_{\mathrm{cm},i}p_{\mathrm{cm},i}^2$ of counter-masses i about joints A_i, the inertias $I_{\mathrm{act},i}$ of actuators i, and the inertias of the equivalent masses $m_{\mathrm{eq},i1} = m_{i2}(1 - p_{i2}/l_{i2})$ of links $i2$ that are modeled in joints B_i as shown in Figure 4(b). From equation (5) $\ddot{\overline{q}}$ can be derived as

$$\begin{aligned} &\frac{\mathrm{d}}{\mathrm{d}t}(\overline{X}_n\dot{\overline{q}}) = \frac{\mathrm{d}}{\mathrm{d}t}(\overline{Y}_n\dot{\overline{u}}) \\ &\frac{\mathrm{d}\overline{X}_n}{\mathrm{d}t}\dot{\overline{q}} + \overline{X}_n\ddot{\overline{q}} = \frac{\mathrm{d}\overline{Y}_n}{\mathrm{d}t}\dot{\overline{u}} + \overline{Y}_n\ddot{\overline{u}} \\ &\ddot{\overline{q}} = (\overline{X}_n)^{-1}\left(\frac{\mathrm{d}\overline{Y}_n}{\mathrm{d}t}\dot{\overline{u}} + \overline{Y}_n\ddot{\overline{u}} - \frac{\mathrm{d}\overline{X}_n}{\mathrm{d}t}\dot{\overline{q}}\right) \end{aligned} \tag{14}$$

with

$$\frac{\mathrm{d}\overline{X}_n}{\mathrm{d}t} = \begin{bmatrix} -l_{11}c(\theta_{11} - \theta_{12})(\dot{\theta}_{11} - \dot{\theta}_{12}) & 0 & 0 & 0 \\ 0 & -l_{21}c(\theta_{21} - \theta_{22})(\dot{\theta}_{21} - \dot{\theta}_{22}) & 0 & 0 \\ 0 & 0 & -l_{31}c(\theta_{31} - \theta_{32})(\dot{\theta}_{31} - \dot{\theta}_{32}) & 0 \\ 0 & 0 & 0 & -l_{41}c(\theta_{41} - \theta_{42})(\dot{\theta}_{41} - \dot{\theta}_{42}) \end{bmatrix} \tag{15}$$

$$\frac{\mathrm{d}\overline{Y}_n}{\mathrm{d}t} = \begin{bmatrix} -s(\theta_{12})\dot{\theta}_{12} & c(\theta_{12})\dot{\theta}_{12} & s(\theta_{12} - \theta_5)(\dot{\theta}_{12} - \dot{\theta}_5)b \\ -s(\theta_{22})\dot{\theta}_{22} & c(\theta_{22})\dot{\theta}_{22} & s(\theta_{22} - \theta_5)(\dot{\theta}_{22} - \dot{\theta}_5)b \\ -s(\theta_{32})\dot{\theta}_{32} & c(\theta_{32})\dot{\theta}_{32} & -s(\theta_{32} - \theta_5)(\dot{\theta}_{32} - \dot{\theta}_5)b \\ -s(\theta_{42})\dot{\theta}_{42} & c(\theta_{42})\dot{\theta}_{42} & -s(\theta_{42} - \theta_5)(\dot{\theta}_{42} - \dot{\theta}_5)b \end{bmatrix}. \tag{16}$$

The angular velocities $\dot{\overline{q}}_2 = [\dot{\theta}_{12}, \dot{\theta}_{22}, \dot{\theta}_{32}, \dot{\theta}_{42}]^T$ of links $i2$ can be obtained from $l_{i2}\dot{\theta}_{i2} = -v_{t,i}^B + v_{t,i}^C$ with the velocity vectors $v_{t,i}^B$ and $v_{t,i}^C$ of joints B_i and C_i normal to line B_iC_i, respectively, as illustrated in Figure 4(a). In matrix notation this is written as

$$\bar{l}_2\dot{\bar{q}}_2 = -\overline{X}_t\dot{\overline{q}} + \overline{Y}_t\dot{\overline{u}} \;\Rightarrow\; \dot{\bar{q}}_2 = (\bar{l}_2)^{-1}(-\overline{X}_t\dot{\overline{q}} + \overline{Y}_t\dot{\overline{u}}) \tag{17}$$

with

$$\bar{l}_2 = \begin{bmatrix} l_{12} & 0 & 0 & 0 \\ 0 & l_{22} & 0 & 0 \\ 0 & 0 & l_{32} & 0 \\ 0 & 0 & 0 & l_{42} \end{bmatrix} \overline{X}_t = \begin{bmatrix} l_{11}c(\theta_{11} - \theta_{12}) & 0 & 0 & 0 \\ 0 & l_{21}c(\theta_{21} - \theta_{22}) & 0 & 0 \\ 0 & 0 & l_{31}c(\theta_{31} - \theta_{32}) & 0 \\ 0 & 0 & 0 & l_{41}c(\theta_{41} - \theta_{42}) \end{bmatrix} \tag{18}$$

and

$$\overline{Y}_t = \begin{bmatrix} -s(\theta_{12})\,c(\theta_{12}) & s(\theta_{12} - \theta_5)\,b \\ -s(\theta_{22})\,c(\theta_{22}) & s(\theta_{22} - \theta_5)\,b \\ -s(\theta_{32})\,c(\theta_{32}) & -s(\theta_{32} - \theta_5)\,b \\ -s(\theta_{42})\,c(\theta_{42}) & -s(\theta_{42} - \theta_5)\,b \end{bmatrix}. \tag{19}$$

The actuator torques $\overline{\tau}_{II}$ are then written as

$$\overline{\tau}_{II} = \overline{M}_{II}(\overline{X}_n)^{-1}\left(\frac{\mathrm{d}\overline{Y}_n}{\mathrm{d}t}\dot{\overline{u}} + \overline{Y}_n\ddot{\overline{u}} - \frac{\mathrm{d}\overline{X}_n}{\mathrm{d}t}\dot{\overline{q}}\right). \tag{20}$$

4.1.3. Actuator torques $\overline{\tau}_{III}$ for the rotational motion of links $i2$ The actuator torques for motion of the mass of links $i2$ is included in $\overline{\tau}_I$ and $\overline{\tau}_{II}$ with the equivalent masses in Figure 4(b). Then also a specific inertia of links $i2$ is included, which is the inertia of the equivalent model about its CoM calculated as $m_{\mathrm{eq},i1}p_{i2}^2 + m_{\mathrm{eq},i2}(l_{i2} - p_{i2})^2$. In general the real inertia of links $i2$ will not be equal to this value. This means that actuator torques $\overline{\tau}_{III}$ are required for the difference in the real inertia and the modeled inertia of links $i2$, which can be written in the mass matrix $\overline{M}_{III}$ as

$$\overline{M}_{III} = \begin{bmatrix} I_{12} - m_{\mathrm{eq},11}p_{12}^2 - m_{\mathrm{eq},12}(l_{12} - p_{12})^2 & 0 & 0 & 0 \\ 0 & I_{22} - m_{\mathrm{eq},21}p_{22}^2 - m_{\mathrm{eq},22}(l_{22} - p_{22})^2 & 0 & 0 \\ 0 & 0 & I_{32} - m_{\mathrm{eq},31}p_{32}^2 - m_{\mathrm{eq},32}(l_{32} - p_{32})^2 & 0 \\ 0 & 0 & 0 & I_{42} - m_{\mathrm{eq},41}p_{42}^2 - m_{\mathrm{eq},42}(l_{42} - p_{42})^2 \end{bmatrix}. \tag{21}$$

The torques $\overline{\Gamma} = [\Gamma_1, \Gamma_2, \Gamma_3, \Gamma_4]^T$ that act on links $i2$ for rotational motion of this difference can be written as

$$\overline{\Gamma} = \overline{M}_{III}\ddot{\overline{q}}_2 \tag{22}$$

with angular accelerations $\ddot{\overline{q}}_2 = [\ddot{\theta}_{12}, \ddot{\theta}_{22}, \ddot{\theta}_{32}, \ddot{\theta}_{42}]^T$ of links $i2$ which can be derived from equation (17) as

$$\begin{aligned} \frac{\mathrm{d}}{\mathrm{d}t}(\bar{l}_2\dot{\bar{q}}_2) &= \frac{\mathrm{d}}{\mathrm{d}t}(-\overline{X}_t\dot{\overline{q}} + \overline{Y}_t\dot{\overline{u}}) \Rightarrow \ddot{\bar{q}}_2 \\ &= (\bar{l}_2)^{-1}\left(-\frac{\mathrm{d}\overline{X}_t}{\mathrm{d}t}\dot{\overline{q}} - \overline{X}_t\ddot{\overline{q}} + \frac{\mathrm{d}\overline{Y}_t}{\mathrm{d}t}\dot{\overline{u}} + \overline{Y}_t\ddot{\overline{u}}\right) \end{aligned} \tag{23}$$

with

$$\frac{\mathrm{d}\overline{X}_t}{\mathrm{d}t} = \begin{bmatrix} -l_{11}s(\theta_{11} - \theta_{12})(\dot{\theta}_{11} - \dot{\theta}_{12}) & 0 & 0 & 0 \\ 0 & -l_{21}s(\theta_{21} - \theta_{22})(\dot{\theta}_{21} - \dot{\theta}_{22}) & 0 & 0 \\ 0 & 0 & -l_{31}s(\theta_{31} - \theta_{32})(\dot{\theta}_{31} - \dot{\theta}_{32}) & 0 \\ 0 & 0 & 0 & -l_{41}s(\theta_{41} - \theta_{42})(\dot{\theta}_{41} - \dot{\theta}_{42}) \end{bmatrix} \tag{24}$$

and

$$\frac{\mathrm{d}\overline{Y}_t}{\mathrm{d}t} = \begin{bmatrix} -c(\theta_{12})(\dot{\theta}_{12}) & -s(\theta_{12})(\dot{\theta}_{12}) & c(\theta_{12} - \theta_5)(\dot{\theta}_{12} - \dot{\theta}_5)b \\ -c(\theta_{22})(\dot{\theta}_{22}) & -s(\theta_{22})(\dot{\theta}_{22}) & c(\theta_{22} - \theta_5)(\dot{\theta}_{22} - \dot{\theta}_5)b \\ -c(\theta_{32})(\dot{\theta}_{32}) & -s(\theta_{32})(\dot{\theta}_{32}) & -c(\theta_{32} - \theta_5)(\dot{\theta}_{32} - \dot{\theta}_5)b \\ -c(\theta_{42})(\dot{\theta}_{42}) & -s(\theta_{42})(\dot{\theta}_{42}) & -c(\theta_{42} - \theta_5)(\dot{\theta}_{42} - \dot{\theta}_5)b \end{bmatrix}. \tag{25}$$

Downloaded from ijr.sagepub.com at Universiteit Twente on June 7, 2013

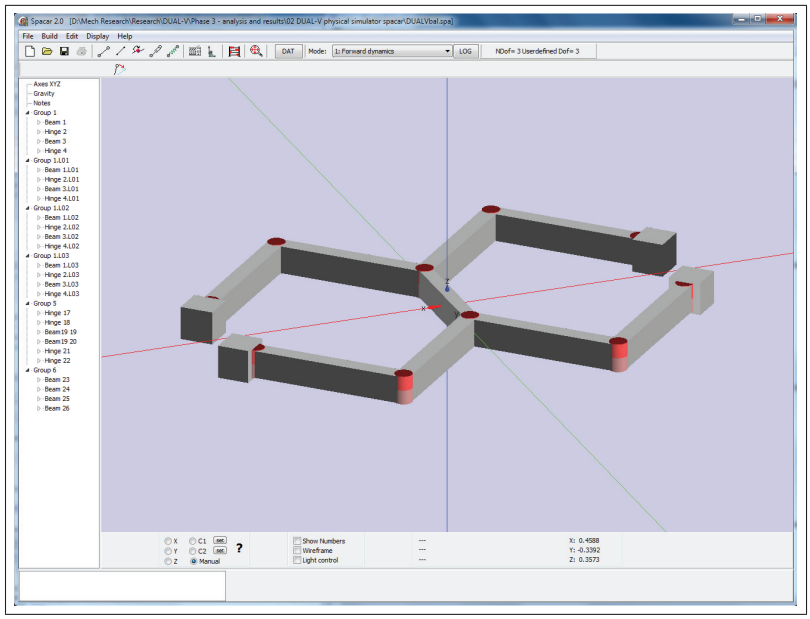

Fig. 5. Spacar model of the balanced DUAL-V manipulator with the mass and inertia modeled in the nodes.

The torque Γ_i on each link l_{i2} can be modeled with forces F_i in both B_i and C_i normal to line B_iC_i as illustrated in Figure 4(c). These forces are calculated with

$$\overline{F}_{III} = (\bar{l}_2)^{-1}\,\overline{\Gamma} \tag{26}$$

with $\overline{F}_{III} = [F_1, F_2, F_3, F_4]^T$. These forces determine the required actuator torques $\overline{\tau}_{III}$ and can be calculated in two parts. The forces F_i in B_i cause a direct torque on the actuators which is written as

$$\overline{\tau}^a_{III} = -\overline{X}_t \overline{F}_{III}. \tag{27}$$

The forces F_i in C_i act on the platform and therefore they can be distributed among the actuators with $\overline{J}^{T*}$ in a similar way as $\overline{\tau}_I$ was calculated, which results in

$$\overline{\tau}^b_{III} = \overline{J}^{T*}\overline{Y}^T_t \overline{F}_{III}. \tag{28}$$

Altogether, the actuator torques $\overline{\tau}_{III}$ are calculated with

$$\overline{\tau}_{III} = \overline{\tau}^a_{III} + \overline{\tau}^b_{III} = (-\overline{X}_t + \overline{J}^{T*}\overline{Y}^T_t)\,\overline{F}_{III}. \tag{29}$$

4.2. *Simulation and validation of the inverse dynamic model*

The DUAL-V manipulator was modeled with the multi-body simulation software package Spacar (http://www.spacar.nl) and the simulation model is shown in Figure 5. Since all mass and inertia data were modeled in the nodes, the shapes of the elements have no meaning.

Figure 6 shows the simulated motion for validation of the inverse dynamic model and the validation results. At each time step the actuator torques were calculated for a given platform motion and the dynamics were solved with the solver ODE45 (Dormand-Prince), with a maximal step size of 0.0001 s and with a relative tolerance of $1\times e^{-12}$ m. The results show the accuracy of the output platform motion with respect to the input platform motion, which is in the order of the relative tolerance of the solver. The platform motion consisted of accelerations up to 118 m/s^2 in the x-direction, up to 202 m/s^2 in the y-direction and up to 1612 rad/s^2 rotationally.

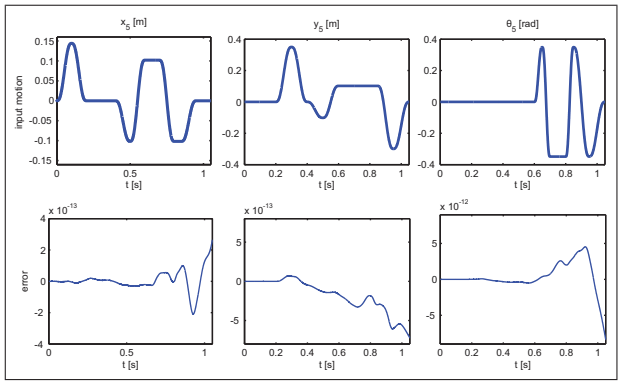

Fig. 6. Validation of the inverse dynamic model for a motion throughout the workspace of the balanced manipulator. The error between the input platform motion and the output platform motion is in the order of the relative tolerance of the solver.

5. Experimental setup

The experimental setup of the prototype manipulator is shown in Figure 7. The manipulator of the aluminium links and brass counter-masses was mounted on four *ETEL RTMB0140-100* direct drive actuators, which could deliver maximal torques of 127 Nm. The actuators were mounted on an aluminium base plate of 1.0 × 0.8 m with a thickness

Downloaded from ijr.sagepub.com at Universiteit Twente on June 7, 2013

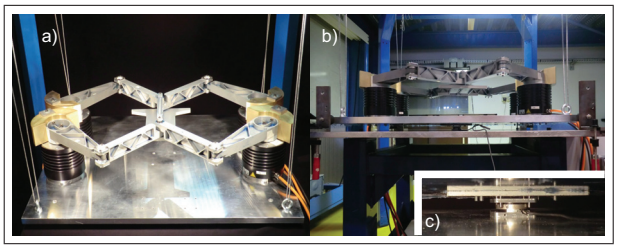

Fig. 7. Experimental setup of the balanced prototype manipulator suspended by cables and mounted on a six-axis force/torque sensor for measurement of the in-plane shaking forces and shaking moment. (a) overview; (b) side view; (c) close-up of sensor mount.

of 25 mm. The unbalanced manipulator for comparison was the same manipulator but without the counter-masses and for evaluation of the sensitivity of the counter-masses on the shaking forces and the shaking moment, the tuning masses of lead were removed from the brass elements.

To measure the shaking forces and the shaking moment of the manipulator in the horizontal plane, an *ATI mini 45* six-axis force/torque sensor was positioned and centered between the base plate and the fixed frame (Figure 7(c)). This sensor could measure a maximum of 500 N shaking force in both x- and y-directions and 20 Nm shaking moment with a measurement noise that was estimated to be about 3 N and 0.02 Nm. To unload the sensor from the gravity force, to align it horizontally, and to prevent damage during assembly, the base plate was suspended by four cables to float just above the sensor. Four pins fixed the sensor with respect to the base plate for in-plane motion while translation in vertical direction was not restricted.

The control of the manipulator was based on a PID-controller at a frequency of 10 kHz. The actuator torques and the actuator orientations were recorded with the same frequency, while the measurement frequency of the force/torque sensor was 1 kHz. With the information from the actuator encoders and the direct kinematic model, the real manipulator motion was determined.

Since at high speeds the PID-controller allowed significant trajectory deviations, to avoid damaging the prototype, the experiments were limited to motion within a centered circular workspace with a diameter of 0.2 m. From Figure 8, which shows the condition number $\kappa = \mathrm{cond}(\overline{J}_\mathrm{h})$ of the harmonized Jacobian matrix $\overline{J}_\mathrm{h} = \overline{J}[1,0,0;0,1,0;0,0,1/b]$ for three platform orientations, it can be observed that within this area the force transmission to the platform is optimal.

6. Experiments and experimental results

In this section the experiments are described and the results are presented. First, various results of the shaking forces and the shaking moment are shown, followed by the results of the actuation torques and the results of the bearing forces. Discussion of the results is in Section 7.

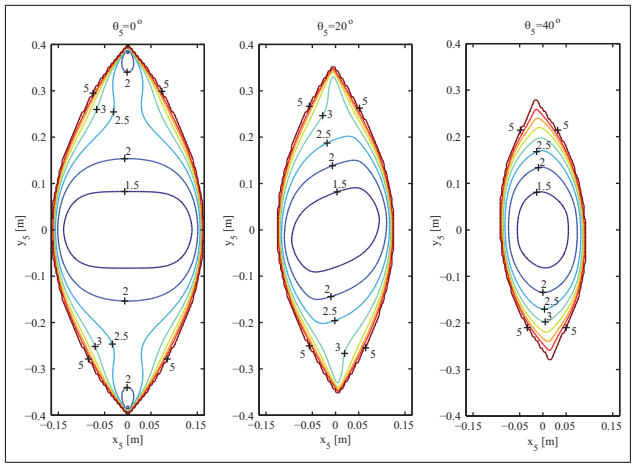

Fig. 8. The condition number throughout the workspace for three platform orientations shows that the optimal dynamic performance is found in the center and along the y-axis.

For motion of the center of the platform along the orthogonal axes and without platform rotation, the unbalanced manipulator is expected to exhibit shaking forces and a zero shaking moment, of which the latter is because of the symmetric design. The balanced manipulator is expected to have zero shaking forces and a zero shaking moment.

Columns 3 and 5 in Figure 9 show the measured shaking forces and shaking moment of the unbalanced and the balanced manipulator, respectively, for the motion shown in column 1, see Extension 1. This motion has a maximal acceleration of 51 m/s^2 in both directions and 43 rad/s^2 rotationally, which therefore is not perfect balanced motion along the orthogonal axes. For validation, the shaking forces and the shaking moment of the unbalanced and the balanced manipulator from simulation of the measured motion are shown in column 2 and 4, respectively.

For motion with a non-rotated platform the unbalanced manipulator can be considered as a reduced mass m_red moving with the platform with which the expected shaking forces can be calculated. This reduced mass can be derived from the force-balance conditions in equations (1) or (2). For the unbalanced manipulator the product $m_{\mathrm{cm},i}p_{\mathrm{cm},i}$ is zero, which can also be interpreted as that the factor $m_5 l_{i1}/2$ is increased with $m_{\mathrm{cm},i}p_{\mathrm{cm},i}$. Then the reduced mass representing the unbalanced manipulator can be obtained from $m_\mathrm{red} l_{i1}/2 = m_{\mathrm{cm},i}p_{\mathrm{cm},i}$ as $m_\mathrm{red} = 2m_{\mathrm{cm},i}p_{\mathrm{cm},i}/l_{i1} = 3.279$ kg. The shaking forces of the unbalanced manipulator in Figure 9 then are expected to be $51 \cdot 3.279 = 167$ N.

A typical motion for pick-and-place tasks including referencing is a motion along a triangular trajectory. Column 1 in Figure 10 shows the measured motion of the manipulator when moved along a triangular trajectory with equal sides of 0.173 m and with maximal accelerations of 66 m/s^2 along x, 63 m/s^2 along y, and 129 rad/s^2 rotationally. For the unbalanced and the balanced manipulator, the shaking forces and the shaking moment from simulation of the measured motion are shown in columns 2 and 4, respectively,

Downloaded from ijr.sagepub.com at Universiteit Twente on June 7, 2013

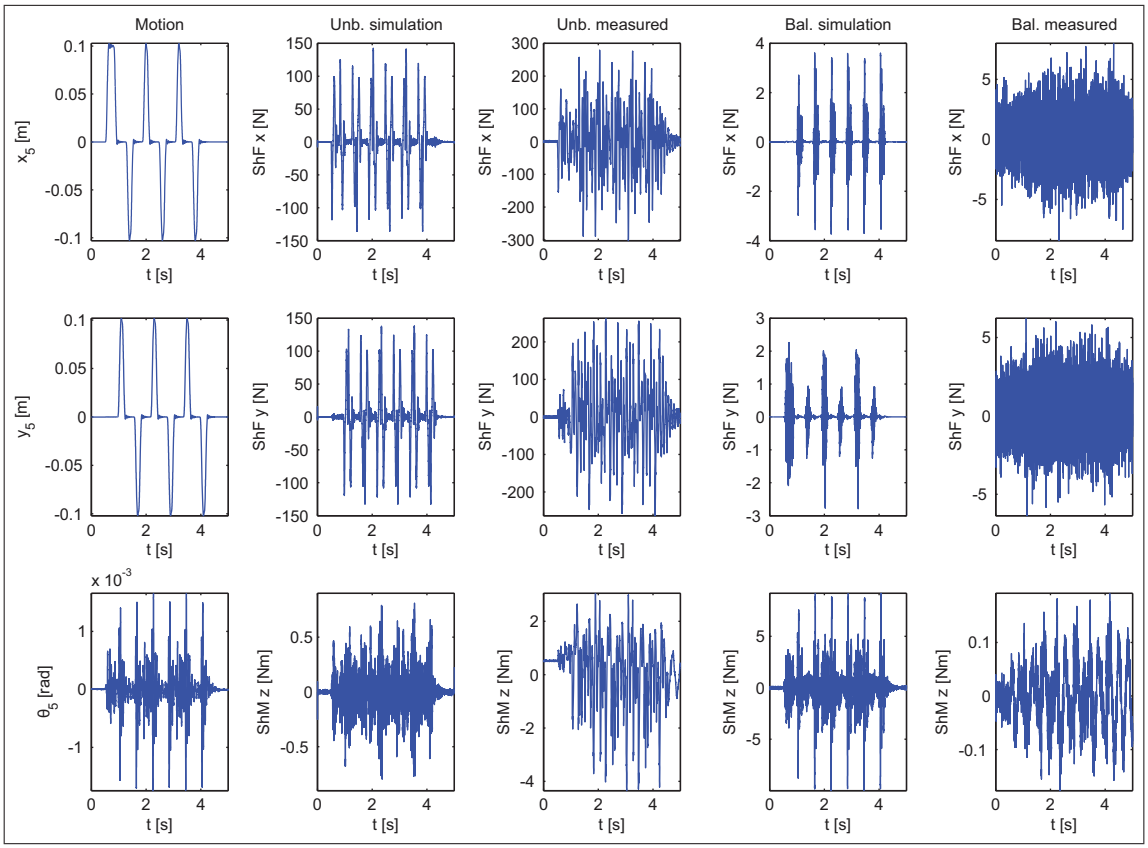

Fig. 9. Results from simulation and experiments of the unbalanced and the balanced manipulator for the measured motion in column 1, which is motion along the orthogonal axes with maximal accelerations of 51 m/s^2 and 43 rad/s^2 rotationally. It shows that the measured shaking forces of the balanced manipulator are 97% and 98% lower in the x- and y-directions, respectively, and the measured shaking moment is 96% lower as compared to the unbalanced manipulator.

and the measured results are shown in columns 3 and 5, respectively. When the platform rotation is zero, the unbalanced manipulator is expected to have shaking forces of $66 \cdot 3.279 = 216$ N along x and $63 \cdot 3.279 = 207$ N along y and the balanced manipulator is expected to exhibit only a shaking moment, while the shaking forces are zero.

To evaluate the sensitivity of the balance masses, the tuning masses were removed from each counter-mass for which each product $m_{\mathrm{cm},i}p_{\mathrm{cm},i}$ is 96.72% of the value for perfect balance, or has a 3.28% balance inaccuracy. Figure 11 shows the experimental results of this 96.72% balanced manipulator and of the fully balanced manipulator for the motion in column 1 which has maximal accelerations of 186 m/s^2 along x, 3 m/s^2 along y, and 50 rad/s^2 rotationally.

The results in Figure 11 also represent the influence of payload on the platform. An equal 3.28% balance inaccuracy is also obtained by placing 0.107 kg in the center of the platform, instead of leaving the tuning masses out. This is calculated similarly as for the reduced mass of the unbalanced manipulator as $2m_{\mathrm{tun},i}p_{\mathrm{tun},i}/l_{i1} = 2 \cdot 0.188 \cdot 0.080/0.280 = 0.107$ kg. By moving this mass with 186 m/s^2 along x, a shaking force of $186 \cdot 0.107 = 20$ N is expected.

For comparison, Figure 12 shows the theoretical simulation results of the inverse dynamic model for the smooth motion along the triangular trajectory of column 1 with maximal accelerations of 82.6 m/s^2 and 71.6 m/s^2 in the x- and y-directions, respectively. The shaking forces and the shaking moment of the unbalanced manipulator, of the 96.72% balanced manipulator, and of the fully balanced manipulator are shown in columns 2, 3 and 4, respectively. Here the shaking forces of the unbalanced manipulator are expected to be $82.6 \cdot 3.279 = 271$ N and $71.6 \cdot 3.279 = 235$ N in the x- and y-directions, respectively, while for the 96.72% balanced manipulator they are expected to be $82.6 \cdot 0.107 = 8.9$ N and $71.6 \cdot 0.107 = 7.7$ N in the x- and y-directions, respectively.

Since the balance masses add inertia to the manipulator, the balanced manipulator is expected to require higher actuator torques. For the motion in Figure 10, the measured actuator torques of the unbalanced manipulator and the balanced manipulator are shown in columns 1 and 2 in Figure 13, respectively. Column 3 shows the actuator torques of both manipulators calculated from the inverse dynamic model for equal input motion. The smaller curves represent the unbalanced manipulator.

Downloaded from ijr.sagepub.com at Universiteit Twente on June 7, 2013

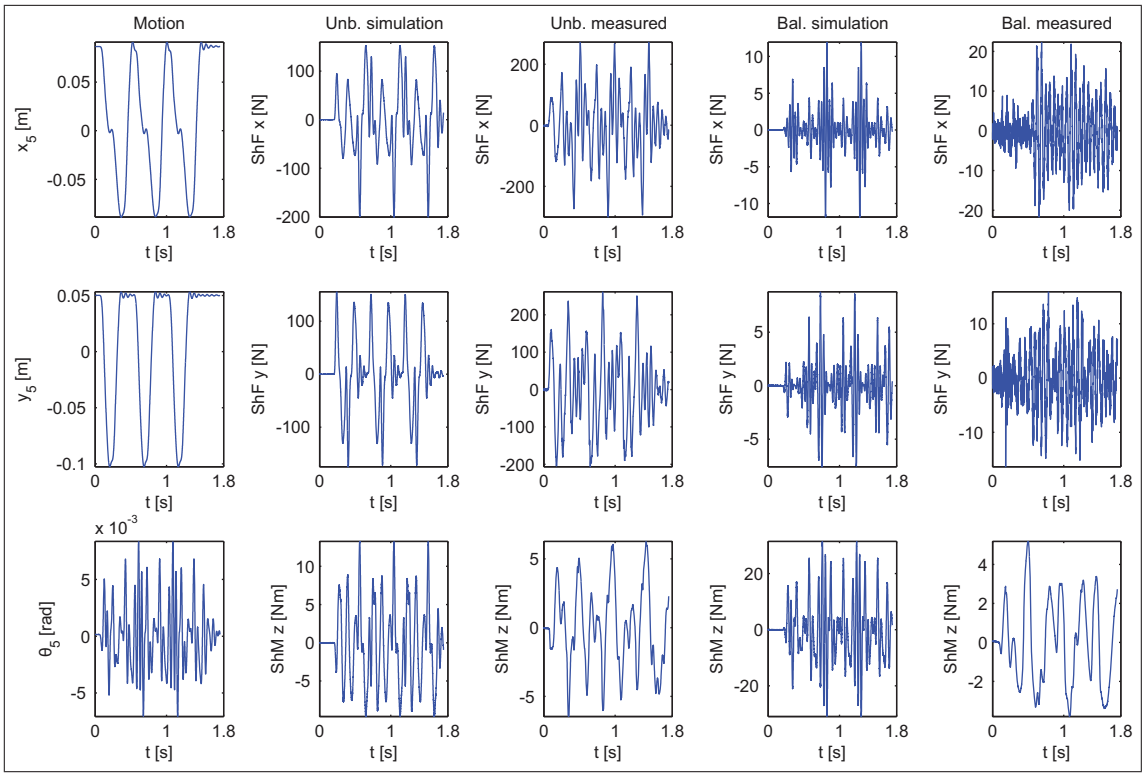

Fig. 10. For the measured motion with maximal accelerations of 66 m/s^2 along x, 63 m/s^2 along y, and 129 rad/s^2 rotationally along a triangular trajectory with equal sides of 0.173 m in column 1, columns 2 and 4 show the simulation results and columns 3 and 5 show the experimental results for the unbalanced and the balanced manipulator, respectively. For the balanced manipulator the measured shaking forces are 93% and 94% lower in the x- and y-directions, respectively, and the measured shaking moment is 16% lower as compared to the unbalanced manipulator.

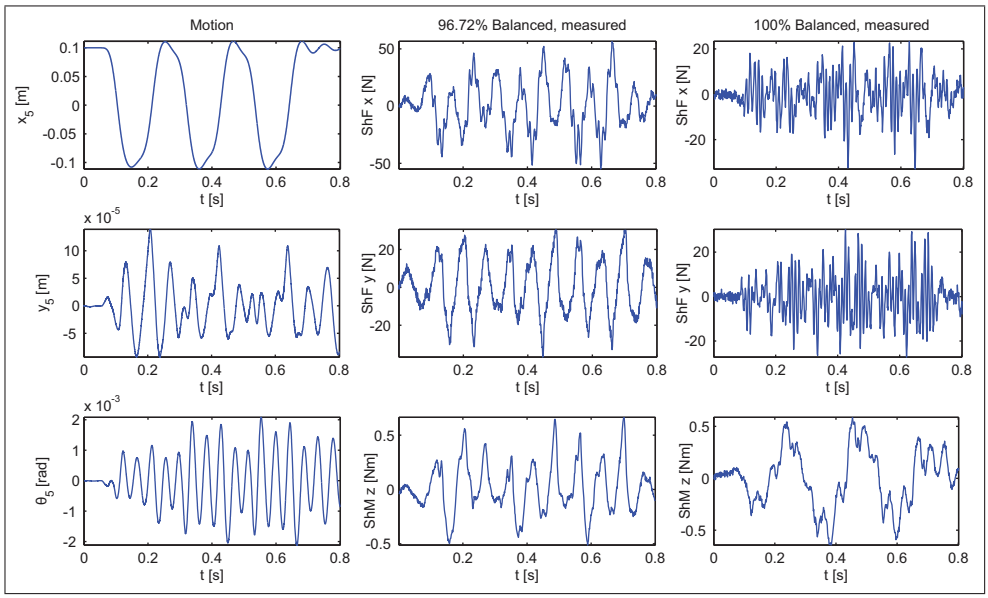

Fig. 11. Experimental results of the 96.72% balanced manipulator and of the fully balanced manipulator for the motion in column 1 with maximal accelerations of 186 m/s^2 along x, 3 m/s^2 along y, and 50 rad/s^2 rotationally. The maximal shaking forces of the 96.72% balanced manipulator are increased with 73% along x and 23% along y, while the maximal shaking moment is reduced with 13%.

Downloaded from ijr.sagepub.com at Universiteit Twente on June 7, 2013

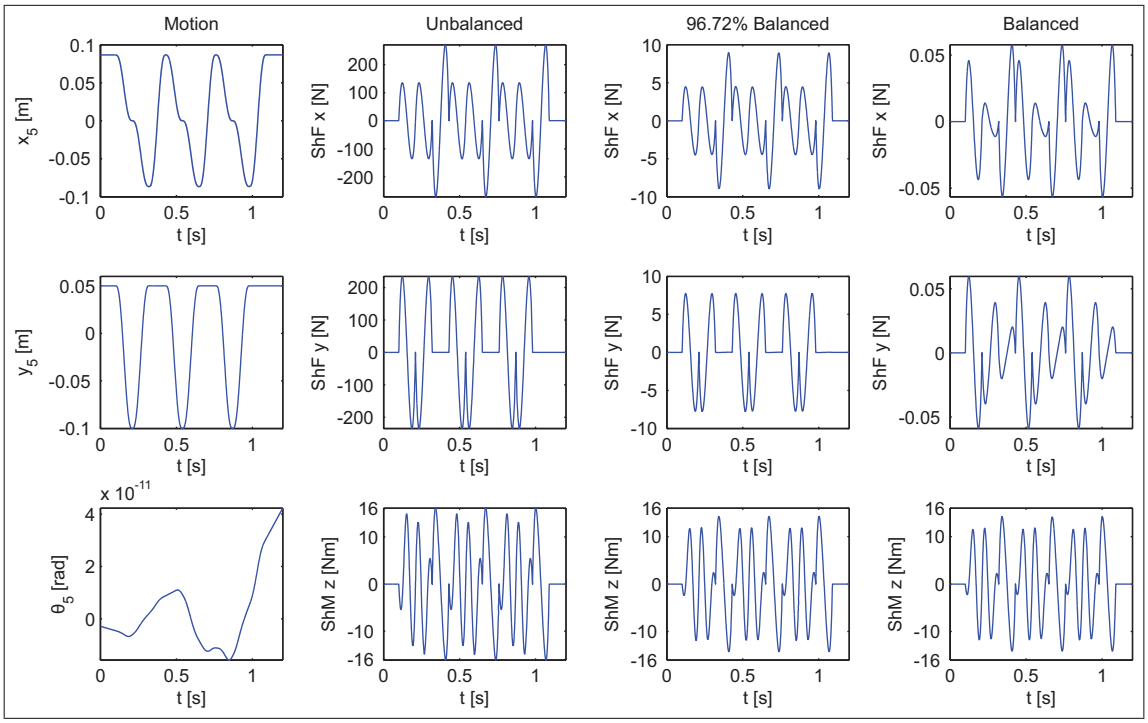

Fig. 12. Theoretical simulation results of the inverse dynamic model of the unbalanced, the 96.72% balanced, and the fully balanced manipulator for the motion in column 1 with maximal accelerations of 82.6 m/s^2 and 71.6 m/s^2 in the x- and y-directions, respectively. 96.72% balance represents 0.107 kg of unbalanced mass on the platform for which the shaking forces increase considerably. The shaking moment of the balanced manipulator is 12% lower as compared to the unbalanced manipulator.

The improved mass distribution due to the countermasses is expected to have an advantageous influence on the bearing forces of the balanced manipulator. For simulations of the measured motion in Figure 10, columns 1 and 2 in Figure 14 show the bearing forces of the unbalanced and the balanced manipulator, respectively. For validation, columns 3 and 4 show the bearing forces from the simulations for smooth motion along the triangular trajectory with equal maximal accelerations.

7. Discussion

In this section the experimental results are discussed. First the shaking forces and the shaking moment are considered and subsequently the sensitivity to unbalance, the actuator torques, and the bearing forces are treated. Also the design approaches and evaluation method are discussed.

7.1. Shaking forces and shaking moments

The measurements in Figure 9 show a significant reduction of the shaking forces of the balanced manipulator. While for the unbalanced manipulator the maximal measured shaking forces are 302 N along x and 263 N along y, the balanced manipulator has maximal shaking forces of 8.4 N along x and 6.4 N along y, being close to the noise level of the sensor. This means a reduction of 97% and 98% of shaking forces along x and y, respectively. The shaking forces of the balanced manipulator are non-zero mainly due to the rotational motion of the platform.

From simulation of the measured motion, the maximal shaking forces of the unbalanced manipulator are about 142 N along x and 138 N along y (column 3) while for the balanced manipulator they are about 3.7 N along x and 2.8 N along y (column 4). Also for these values the reduction of shaking forces is 97% and 98% along x and y, respectively, however the values differ significantly from the measured maximal values. Also both values of the unbalanced manipulator differ from the expected 167 N shaking forces. Most likely this is caused by the calculations of the derivative (velocity) and the second derivative (acceleration) of the measured motion, which are needed for the inverse dynamic model. Since the derivatives of the measured position information result in unrealistically high values, the values were filtered with a first-order low-pass filter. However the simulation results show that this is not sufficient. In addition, the mentioned maximal accelerations were obtained from these derivatives, which explains why the expected shaking forces are closer to the results of the simulation of the measured motion.

The measured shaking moment of the unbalanced manipulator has a maximal value of 4.3 Nm, while for the balanced manipulator it is at most 0.19 Nm, which is 96% lower. It is likely that the measurements of the unbalanced manipulator are affected significantly by frame vibrations.

Downloaded from ijr.sagepub.com at Universiteit Twente on June 7, 2013

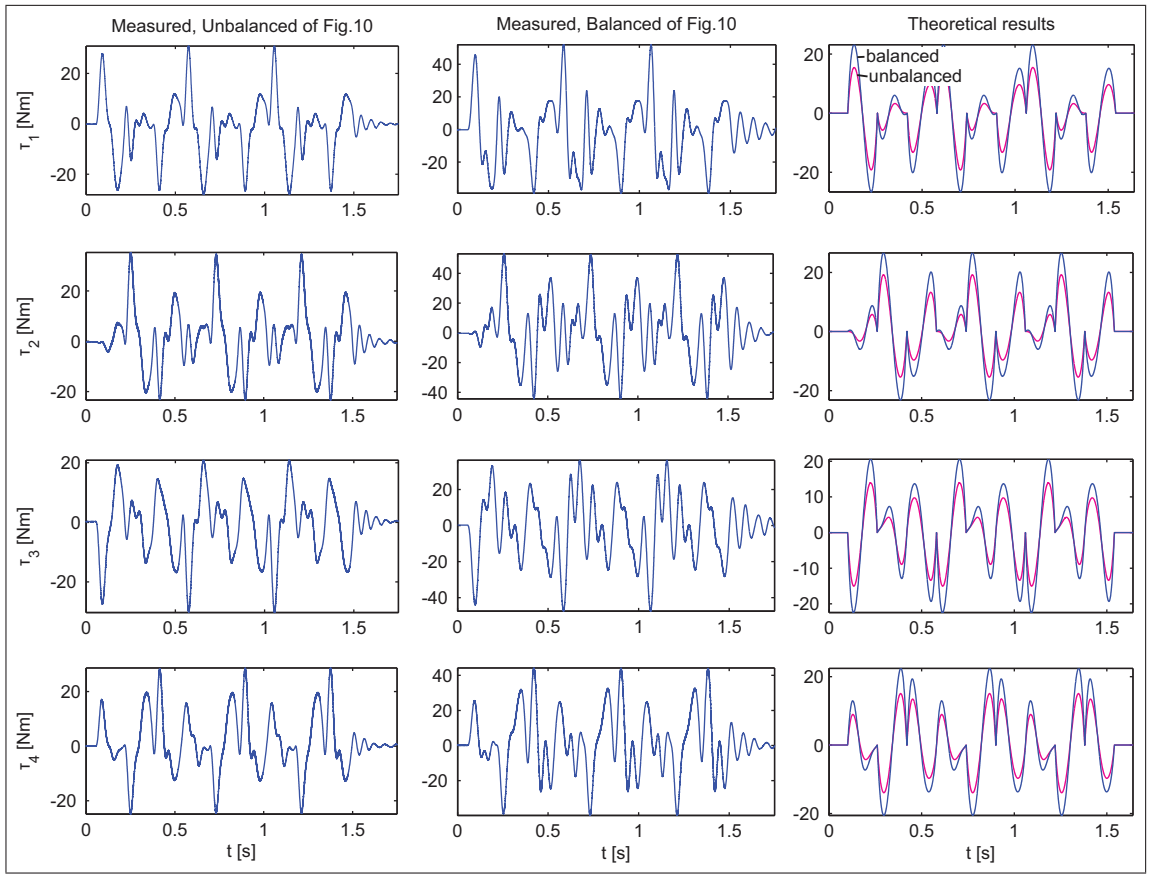

Fig. 13. For the motion in Figure 10 the measured actuator torques of the unbalanced and the balanced manipulator are shown in columns 1 and 2, respectively. Column 3 shows the actuator torques of both manipulators from the inverse dynamic model for equal input motion. The smaller curves represent the unbalanced manipulator. From experiments, the actuator torques of the balanced manipulator are about 1.6× higher while theoretically they are about 1.4× higher than the actuator torques of the unbalanced manipulator.

In the experimental setup the relatively large inertia of the manipulator with the base plate in combination with the stiffness of the force/torque sensor caused the base plate to rotate in the lowest eigenmode with measured eigenfrequency of about 3.4 Hz. This may have caused interference of the relatively high shaking forces with the measured shaking moment.

The simulation results of the shaking moment (columns 2 and 4) are dramatically affected by the mentioned differentiation problem. Although the values of the unbalanced manipulator could be realistic, the values of the balanced manipulator are, with a maximal value of 10 Nm, significantly higher as compared to the measured values. The shaking moment is obtained from the simulation as the sum of the actuator torques together with the moments created by the individual reaction forces in A_i with respect to the center. Due to the differentiation problem, all individual reaction forces are affected for which the resulting shaking moments become useless.

For motion along the triangular trajectory, Figure 10 shows that the measured shaking forces of the balanced manipulator have maximal values of 22 N along x and 16 N along y, which are non-zero because of rotational motion of the platform. Compared with the unbalanced manipulator showing maximal measured shaking forces of 300 N along x and 262 N along y, the balanced manipulator has 93% and 94% reduced shaking forces, respectively. The maximal measured shaking moment of the unbalanced manipulator is 6.5 Nm while of the balanced manipulator it is 5.2 Nm, which is 16% lower.

From the simulations in columns 2 and 4, the unbalanced manipulator has maximal shaking forces of 200 N along x and 175 N along y, while for the balanced manipulator the maximal shaking forces are 12 N along x and 8.8 N along y. This results in 94% and 95% reduced shaking forces along x and y, respectively, for which they differ 1% from the results from the measurements. Regarding the simulated results, the same remarks apply as for Figure 9, for which the simulated shaking moments cannot be interpreted.

From the theoretical simulation of motion along the triangular trajectory in Figure 12, the unbalanced manipulator has maximal shaking forces of 271 N along x and 235 N along y, as expected, while the balanced manipulator has minimal shaking forces. The maximal shaking moment of the unbalanced manipulator is 16.1 Nm while

Downloaded from ijr.sagepub.com at Universiteit Twente on June 7, 2013

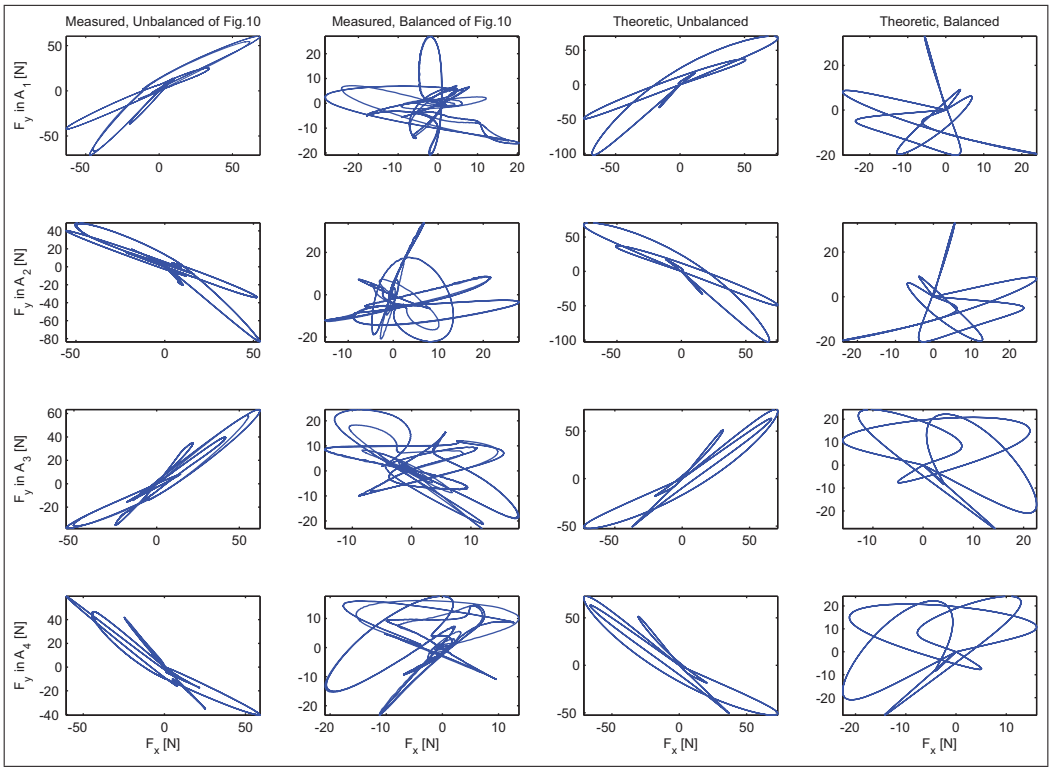

Fig. 14. For the motion in Figure 10, the bearing forces from simulation of the measured motion of the unbalanced and the balanced manipulator are shown in columns 1 and 2, respectively. Columns 3 and 4 show the results from simulation of smooth motion along the triangular trajectory with equal maximal accelerations. It was found that the maximal bearing forces of the balanced manipulator were 73% lower in joints A_1 and A_2 and were 69% lower in joints A_3 and A_4 as compared to the unbalanced manipulator.

the maximal shaking moment of the balanced manipulator is 14.1 Nm which is 12% lower. This is less than the measured difference in maximal shaking moment of 16% in Figure 10.

7.2. Sensitivity

The sensitivity of the dynamic balance was investigated for a balance inaccuracy of 3.28%, representing the effect of inaccurate counter-masses that are 0.188 kg too lightweight or of a payload of 0.107 kg on the platform. The results in Figure 11 show that for 3.28% balance inaccuracy, the shaking forces increase from maximal values of 33 N along x and 30 N along y (column 3) to maximal values of 57 N along x and 37 N along y (column 2). This means an increase of shaking forces of 73% along x and 23% along y. The difference in shaking force along x is $57 - 33 = 24$ N and close to the expected 20 N shaking force for the 3.28% balance inaccuracy. The maximal shaking moment was reduced from 0.64 Nm (column 3) to 0.56 Nm (column 2) which is a reduction of 13%.

The theoretical simulation of motion along the triangular trajectory in Figure 12 shows that the 96.72% balanced manipulator has maximal shaking forces of 8.9 N along x and 7.7 N along y, as expected from the calculations from the force-balance conditions. This means that the expected shaking forces of the manipulator for motion without rotation of the platform can be described as

$$\begin{bmatrix} ShF_x \\ ShF_y \end{bmatrix} = \frac{2(m_{\mathrm{cm},i}p_{\mathrm{cm},i})^{dif}}{l_{i1}} \begin{bmatrix} \ddot{x}_5 \\ \ddot{y}_5 \end{bmatrix} = m_{\mathrm{payload}} \begin{bmatrix} \ddot{x}_5 \\ \ddot{y}_5 \end{bmatrix} \quad (30)$$

showing a linear relation between the shaking forces ShF_x and ShF_y and the balance inaccuracy or difference from perfect balance $(m_{\mathrm{cm},i}p_{\mathrm{cm},i})^{dif}$ and the payload m_{payload} on the platform. The maximal shaking moment of the 96.72% balanced manipulator in Figure 12 is 14.2 Nm, which is, contrary to the measured results, about 1% higher than of the fully balanced manipulator.

Due to the PID-controller that allowed the manipulator to move imperfectly along the desired trajectories, from the results in Figures 9, 10 and 11 the sensitivity to motion inaccuracy is also shown. For imperfect motion along the orthogonal axes, Figure 9 shows that shaking moments exist, however they remain small as compared to the motion in Figure 10. The sensitivity to rotation of the platform is also shown. Small rotations of the platform can already contribute significantly to the shaking forces since the measured shaking forces of the balanced manipulator in Figures 9, 10 and 11 are not zero as expected.

Altogether it can be concluded that small inaccuracies of the counter-masses, of unbalanced payload on the platform, and of platform rotations can lead to considerable vibration

Downloaded from ijr.sagepub.com at Universiteit Twente on June 7, 2013

for high-speed manipulations although they remain significantly low compared to the unbalanced manipulator. Therefore high accuracy in the design, production, and control of a balanced manipulator is important for optimal dynamic balance.

7.3. Actuator torques

The measured actuator torques in Figure 13 show that the torques required to move the balanced manipulator are higher than the torques of the unbalanced manipulator. The maximal values of the torques τ_1, τ_2, τ_3, and τ_4 of the unbalanced manipulator are 31, 35, 30 and 29 Nm, respectively, and of the balanced manipulator they are 52, 53, 47 and 44 Nm, respectively. This means that for the balanced manipulator they are 1.68, 1.51, 1.57, and 1.52× the torques of the unbalanced manipulator, respectively, which is on average 1.6× higher.

From the theoretical results in column 3 in Figure 13, the maximal torques τ_1 and τ_2 are both 1.42× higher being 27 Nm and the maximal torques τ_3 and τ_4 are both 1.47× higher being 22 Nm, which is on average 1.4× higher for the balanced manipulator. The actuator torques from the theoretical results are lower than the measured torques which may be caused by the high torques that the PID-controller calculates to correct the output motion and by friction which was not included in the calculations with the inverse dynamic model.

7.4. Bearing forces

The bearing forces shown in columns 1 and 2 in Figure 14 were derived from the simulation of the real motion in Figure 10. Since the values of the shaking forces from these simulations have been considered to be inaccurate due to the differentiation problem, the values of the individual bearing forces are also inaccurate. However the results from the simulation in Figures 9 and 10 have been shown to be suitable for comparing the unbalanced and the balanced manipulator.

For simulation of precise motion along the triangular trajectory with equal accelerations, columns 3 and 4 of Figure 14 show the bearing forces of which the shapes and sizes are comparable with columns 1 and 2. From both simulations it is found that the maximal bearing forces in A_1 and A_2 are 73% lower and in A_3 and A_4 are 69% lower for the balanced manipulator. The maximal forces were calculated as $\max(\sqrt{F_x^2 + F_y^2})$ in each bearing. The lower bearing forces imply that the balanced manipulator has reduced positioning errors.

7.5. Design approaches and evaluation method

The approaches to the design of balanced manipulators have resulted in a new manipulator which has been shown to be both feasible for high-speed tasks and to have low vibration of its base. The aim was to have a perfectly dynamically balanced manipulator along the orthogonal axes. Since all motion of the manipulator remains in the vicinity of perfect balance, the manipulator has proved to have significant balance performance throughout the workspace.

These design approaches can be applied for the synthesis of other planar and spatial dynamically balanced multi-DoF parallel manipulators. For planar manipulators, the linear momentum equations can be investigated to find the optimal kinematic and dynamic parameters of an initial configuration. This approach may be challenging for spatial manipulators since their linear momentum equations can be complex. Composing spatial manipulators of known balanced architectures may then be more advantageous. To obtain spatial mechanisms with the desired mobility together with optimal similar opposite motions of the masses and inertias, for which advantageous balance solutions are found, remains a challenge of future research.

The evaluation method of considering the measured motion of the manipulator and using this motion as input for the simulations was shown to be partly successful. Since only position data of the manipulator motion were recorded, these data had to be differentiated twice to obtain the velocity data and the acceleration data at each time step. Because of this, the obtained values for the shaking forces and shaking moment were not equal to the measured values. However, the resulting shaking forces from simulations were shown to be applicable for the relative comparison of the balanced and the unbalanced manipulator. This was not true for the shaking moments. Therefore, for a better application of this evaluation method, it is required to have accurate velocity and acceleration data, for example by measuring, in addition to the position, the velocity, and the acceleration of the manipulator motion during experiments with additional sensors.

8. Conclusion

The design of a dynamically balanced redundant planar 4-RRR parallel manipulator was presented together with the design approach of adapting a given kinematic architecture and of composing it from known balanced architectures. A prototype manipulator in an experimental setup was presented for evaluation and comparison of the balanced manipulator with the unbalanced manipulator. A method was proposed for a fair evaluation and comparison in which the measured motion from the experiments was used as input for the simulation. For precise simulation of the manipulator motion, the inverse dynamic model of the manipulator was derived and validated.

The prototype manipulator successfully performed high-speed motion with low base vibration. Experiments showed that the balanced manipulator has about 97% lower shaking forces and a 96% lower shaking moment for motion along the orthogonal axes. For motion throughout the workspace, the balanced manipulator showed about 93% lower shaking

Downloaded from ijr.sagepub.com at Universiteit Twente on June 7, 2013

forces and 16% lower shaking moment. Since the PID-controller allowed small rotational motion of the platform, causing shaking forces, it is expected that these values will reduce further when the control of the rotation of the platform is improved.

A relatively small balance inaccuracy of 3.28%, representing too light counter-masses or an unbalanced payload on the platform, was shown to increase the shaking forces considerably, while they still remain significantly low as compared to the unbalanced manipulator. For a manipulator with optimal dynamic balance, accurate design and production are therefore important. The actuator torques of the balanced manipulator were shown to be about 1.6× higher than for the unbalanced manipulator and the bearing forces of the balanced manipulator were shown to be about 71% lower than for the unbalanced manipulator.

It was found that shaking forces and shaking moments obtained from precise simulation of the measured manipulator motion with the inverse dynamic model are affected by the differentiation of the measured position data to obtain velocities and accelerations. The obtained values were shown to be useful for the relative comparison of the shaking forces of the balanced and the unbalanced manipulator, but their values were not equal to the measured values.

Funding

This work was partially funded by the French Funding Agency for Research ANR-ARROW project.

References

Agrawal SK, Gardner G and Pledgie S (2001) Design and fabrication of an active gravity balanced planar mechanism using auxiliary parallelograms. *Journal of Mechanical Design* 123: 525–528.

Arakelian VG and Smith MR (2005a) Shaking force and shaking moment balancing of mechanisms: A historical review with new examples. *Journal of Mechanical Design* 127: 334–339.

Arakelian VH and Smith MR (2005b) Erratum: Shaking force and shaking moment balancing of mechanisms: A historical review with new examples. *Journal of Mechanical Design* 127: 1035.

Briot S, Arakelian VH and Guégan S (2009) PAMINSA: A new family of partially decoupled parallel manipulators. *Mechanism and Machine Theory* 44: 425–444.

Chung WK and Cho HS (1988) On the dynamic characteristics of a balanced PUMA-760 robot. *Industrial Electronics* 35: 222–230.

Corbel D, Gouttefarde M, Company O and Pierrot F (2010) Towards 100G with PKM. Is actuation redundancy a good solution for pick-and-place? *IEEE international conference on robotics and automation (ICRA '10)*, Anchorage, USA, 22–28 April 1996, pp. 4675–4682. Piscataway: IEEE Press.

Demeulenaere B and Berkof RS (2008) Improving machine drive dynamics: A structured design approach toward balancing. *Journal of Mechanical Design* 130: 082302.

Fischer O (1906) *Theoretische Grundlagen für Eine Mechanik der Lebenden Körper*. Leipzig: Teubner.

Foucault S and Gosselin CM (2004) Synthesis, design, and prototyping of a planar three degree-of-freedom reactionless parallel mechanism. *Journal of Mechanical Design* 126: 992–999.

Jean M and Gosselin CM (1996) Static balancing of planar parallel manipulators. *IEEE international conference on robotics and automation (ICRA '96)*, Minneapolis, MN, USA, 22–28 April 1996, pp. 3732–3737. Piscataway: IEEE Press.

Lim TG, Cho HS and Chung WK (1989) A parameter identification method for robot dynamic models using a balancing mechanism. *Robotica* 7: 327–337.

Lim TG, Cho HS and Chung WK (1990) Payload capacity of balanced robotic manipulators. *Robotica* 8: 117–123.

Ricard R and Gosselin CM (2000) On the development of reactionless parallel manipulators. *ASME international design engineering technical conference and the computer Information engineering conference (DETC '00)*, Baltimore, MD, USA, 10–14 September 2000, article no. 14098.

Van der Wijk V, Demeulenaere B, Gosselin C and Herder JL (2012) Comparative analysis for low-mass and low-inertia dynamic balancing of mechanisms. *Mechanisms and Robotics* 4: 031008.

Van der Wijk V and Herder JL (2008) Dynamic balancing of mechanisms by using an actively driven counter-rotary counter-mass for low mass and low inertia. *2nd international workshop on fundamental issues and future research directions for parallel mechanisms and manipulators*, Montpellier, France, 21–22 September 2008, pp. 241–251.

Van der Wijk V and Herder JL (2009) Guidelines for low mass and low inertia dynamic balancing of mechanisms and robotics. In: Kröger T and Wahl FM (eds) *Advances in Robotics Research*. New York: Springer, pp. 21–30.

Van der Wijk V and Herder JL (2012a) Inherently balanced 4R four-bar based linkages. In: Lenarčič J and Husty M (eds) *Latest Advances in Robot Kinematics*. New York: Springer, pp. 309–316.

Van der Wijk V and Herder JL (2012b) Synthesis method for linkages with center of mass at invariant link point - pantograph based mechanisms. *Mechanism and Machine Theory* 48: 15–28.

Van der Wijk V, Herder JL and Demeulenaere B (2009) Comparison of various dynamic balancing principles regarding additional mass and additional inertia. *Mechanisms and Robotics* 1: 041006.

Van der Wijk V, Krut S, Pierrot F and Herder JL (2011) Generic method for deriving the general shaking force balance conditions of parallel manipulators with application to a redundant planar 4-RRR parallel manipulator. In: *13th IFToMM world congress on mechanism and machine science*, Guanajuato, Mexico, article no. A12-523.

Appendix: Index to Multimedia Extensions

The multimedia extension page is found at http://www.ijrr.org.

Table of Multimedia Extensions

Extension	Type	Description
1	Video	Unbalanced and balanced motion of the DUAL-V manipulator

Downloaded from ijr.sagepub.com at Universiteit Twente on June 7, 2013